Vector intensity measures for a more accurate reliability assessment of NPP sub-systems

Pierre Gehl, Jeremy Rohmer

TINCE 2018 – Technological Innovations in Nuclear Civil Engineering
France, Paris-Saclay – 2018, August 29 | 31

87. Vector intensity measures for a more accurate reliability assessment of NPP sub-systems

Pierre Gehl [1*], Jeremy Rohmer [1]

[1] BRGM, Direction Risques et Prévention, Orléans, France
[*] Corresponding Author, E-mail: p.gehl@brgm.fr

Within the European-funded H2020 NARSIS project, one of the main challenges pertains to the development of innovative methods for the numerical derivation of fragility functions for systems, structures or components (SSCs) within nuclear power plants (NPPs). In this context, the present study investigates the effect of integrating secondary seismic intensity measures when assessing the reliability of SSCs, with the objective of better identifying or even reducing the uncertainties due to record-to-record variability. While such an approach has already been applied to common reinforced-concrete or masonry buildings in previous studies, it is proposed here to consider an industrial structure containing a set of components at various locations of the building. We propose to treat the problem of station blackout following an earthquake: the internal equipment is supposed to perform a given function (e.g., generation of emergency on-site power) and it may therefore be considered as a sub-system, for which a functionality assessment may be required within a probabilistic safety analysis. The studied sub-system comprises various types of components, whose failure modes are susceptible to either floor acceleration spectra or inter-story drift. Such engineering demand parameters at various floor locations are not evenly correlated with the same intensity measures (e.g., spectral accelerations at different periods), thus highlighting the need for vector intensity measures that are able to capture a wide range of potential failure modes. Finally, the vector-based fragility functions derived at the component level are assembled in order to quantify the probability of the sub-system losing its function, for various levels of seismic loading. The statistical dependence between component failure events is taken into account thanks to system reliability techniques.

KEYWORDS: seismic hazard, system reliability, fragility functions, Bayesian networks

Introduction

Recent events, such as the Fukushima Daichi NPP accident in 2011 or the 2007 Chūetsu-oki earthquake leading to incidents at the Kashiwazaki-Kariwa NPP, have shown the need for a more accurate estimation of the impact of external hazard loadings on nuclear installations. Therefore, the European-funded H2020 NARSIS (New Approach to Reactor Safety ImprovementS, http://narsis.brgm.fr) proposes to improve all the elements that usually involved in Probabilistic Safety Assessment procedures (PSAs), from the probabilistic characterization of natural hazards to the risk integration of possible interactions and cascading effects. More specifically, an essential task in PSAs consists in the vulnerability estimation of the structures, systems and components (SSCs) within NPPs, through fragility curves that express the probability of an SSC to reach or exceed a predefined damage state as a function of an intensity measure representing the hazard loading. Their probabilistic nature make them well suited for PSA applications, at the interface between probabilistic hazard assessments and event tree analyses, in order to estimate the occurrence rate of undesirable top events.
Due the high number and variety of SSCs, most of these fragility models are evaluated with simplified procedures such as the safety factors approach, as summarized in Zentner et al. (2017). However, with a more selective screening of critical SSCs and the constant improvement of computational capacities, it becomes feasible to derive specific fragility models through numerical simulations in the case more

accurate failure estimations are needed. Therefore, one of the main objectives of the NARSIS project is to build vector-based fragility models that use more than one intensity measure (IM), in order to account for a wide range of loading types in a multi-hazard context. In the specific case of fragility curves for seismic hazard, it has been shown that a single IM is neither sufficient nor efficient in order to represent the complexity of an earthquake ground-motion time-history (Gehl et al., 2013). Previous studies applied to reinforced-concrete or masonry structures (Modica & Stafford, 2014; Sousa et al., 2014) have proven the benefit of using composite IMs, mostly as a way to reduce the dispersion of the fragility model (i.e., the "slope" of the cumulative distribution functions). However, in the specific case of NPPs where some SSCs may be seen as sub-systems that are required to perform a given function, the components within the studied sub-system (e.g., structural elements or internal equipment) are not sensitive to the same types of IMs (e.g., different frequency ranges). Moreover, their seismic responses may not be evaluated with the same type of engineering demand parameters (EDPs), since the damage state of some components is linked to the amount of deformation sustained or the peak floor acceleration. In this context, the use of vector-based fragility models would then prove very valuable in order to capture accurately the relations between the various couples of IMs and EDPs. Therefore, it is proposed to investigate the derivation of such fragility models applied to a sub-system of SSCs, and to investigate their potential benefit over single-IM fragility curves.

First, a simplified case of a sub-system is characterized: it consists in a 5-story structure containing internal equipment (i.e., two emergency diesel generators located at different floors). The generators are assumed to be part of the on-site power generation system, in the case of off-site power loss (see Figure 1). This sub-system is an essential component of the chain of events potentially leading to a station blackout event, which is acknowledged as one of the critical incidents that may trigger the loss of the control systems of an NPP (e.g. the flooding of the emergency generators that led to a station blackout and ultimately to the Fukushima NPP accident). The fragility functions are then derived from a set of non-linear time-history analyses (NLTHA), for which natural ground-motion records are selected following the conditional spectrum procedure. The fragility functions for the different components (i.e., structural system and emergency generators) are then assembled into a fragility model for the whole sub-system, thanks to a Bayesian Network formulation (Gehl & D'Ayala, 2016). Finally, the statistical robustness of the proposed vector-based fragility model is discussed and compared to other fragility functions that use scalar or vector-IMs at various stages of the procedure.

Modelling of an on-site emergency power sub-system

The occurrence of station blackouts has been the object of many studies (NUREG, 2005), which have identified a wide range of SSCs that may be involved in the chain of events leading to off-site and on-site power loss (e.g., buses, relays, switchgears, diesel generators, etc.). For illustration purposes, it is proposed here to consider a simplified sub-system with a reinforced-concrete structure hosting two emergency diesel generators (EDGs), for the delivery of backup on-site power in case the off-site power grid is lost.

The proposed building corresponds to the structural model detailed in Pisharady and Basu (2009), which consists of a 2-D 5-story reinforced-concrete frame structure (see Figure 1). It is assumed that the two EDGs are located at the 2nd and 4th stories, respectively. The structure is modelled with the OpenSees platform (McKenna et al., 2000), using fiber elements to represent the sections of the beams and columns. Another simplification lies in the use of a fixed-based model, while soil-structure interactions are left out of the scope of the study, pending further developments of specific models.

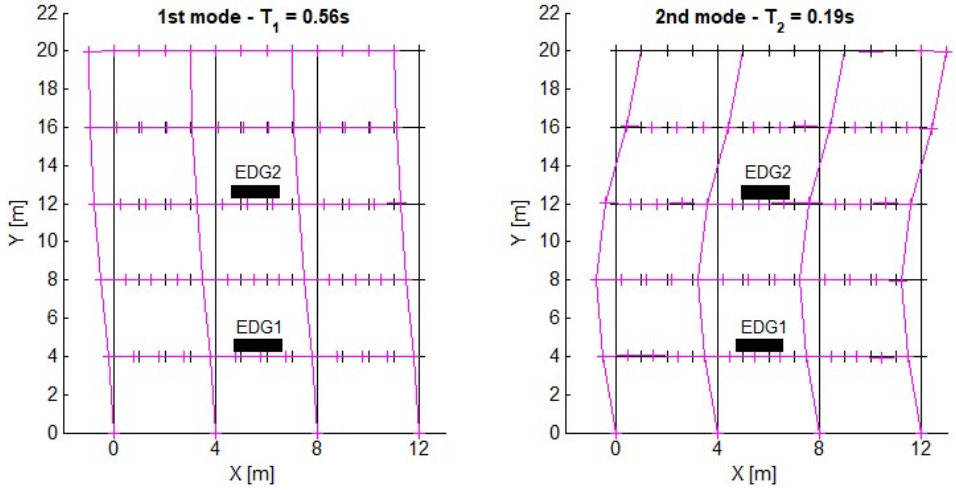

Figure 1: Layout of the 2-D structural model and location of the EDGs (black rectangles). The deformed shapes represent the first two modes of vibration of the structure.

The EDGs are not explicitly modelled and their contribution to the structural system is accounted for by adding larger masses to the 2nd and 4th stories. As a result, the modal analysis of the structure identifies the first two modes of vibration (see Figure 1) at periods T_1 = 0.56s and T_2 = 0.19s. For deriving fragility functions, the structural system is then subjected to a series of ground motions: during the NLTHA, the behavior of the structure is assessed by using the maximum transient inter-story drift ratio (*ISDR*) as the EDP. On the other hand, the EDGs are considered as rigid blocks, for which one of the main failure modes is the rupture of the anchor bolts through concrete coning for instance (Choun et al., 2007; Wang, 2015): therefore the peak floor accelerations (*PFA*) at stories 2 and 4 constitute suitable EDPs. The limit states for the three damage events (*STR* for structural damage and *EDG* for failure of the anchorage of the EDGs) are provided in Table 1: they have been estimated so that they correspond to the apparition of yielding behaviour for *STR*, and to the concrete breakout for EDG anchors in tension.

Component	EDP	Limit state	Functional role in the system
STR	Max. *ISDR*	1.5 %	Structural damage is assumed to stop all operations
EDG1	*PFA* (Story 2)	8 m/s^2	At least 1-out-of-2 EDGs is required to generate on-site power
EDG2	*PFA* (Story 4)	8 m/s^2	

Table 1: **Description of the NPP components considered for the on-site emergency power sub-system.**

Ground-motion selection

Since one of the objective of this study is to assess the relevance of vector-based fragility functions with respect to single-IM fragility curves, it is necessary to adopt a rigorous framework for the selection of the ground-motion records to be used in the NLTHA, in order to avoid combinations of IM values that are not compatible with the studied site. To this end, the ground-motion selection procedure based on the conditional spectrum, proposed by Lin et al. (2013) is applied here. This approach enables the scaling of ground-motions records while preserving the hazard consistency of the target response spectrum. The main steps of this procedure are the following:

- Probabilistic hazard assessment of the studied site: here, an arbitrary location in Southern Europe is selected, assuming stiff soil conditions with $V_{s,30}$ = 600 m/s. Hazard curves are generated with the OpenQuake platform (www.globalquakemodel.org), accounting for 13 seismogenic areas which have been characterized in the SHARE project (Woessner et al., 2013).
- Selection of a period of interest and of scaling levels: here, the response spectrum is chosen to be conditioned on $SA(T_1$=0.56s), with 10 scaling levels ranging from 0.87 m/s^2 to 15.22 m/s^2, corresponding to return periods from 43 years to 19 900 years.

- Identification of reference earthquakes: for the studied site, the OpenQuake software is used to perform a hazard disaggregation for each scaling level. A reference earthquake scenario may then be defined by the variables [M_w; R_{jb}; ε] (magnitude, Joyner-Boore distance, epsilon of the ground-motion prediction equation), which are averaged from the disaggregation results (Bazzurro and Cornell, 1999).
- Generation of the target response spectrum for each scaling level and reference earthquake scenario, and selection of compatible ground-motion records using the algorithm by Jayaram et al. (2011). The final selection from the PEER database (PEER, 2013) consists of 30 records for each of the 10 scaling levels (i.e., 300 ground-motion records in total).

As a result, the mean conditional spectra for the 10 scaling levels, as well as the response spectra of the 300 ground-motion records are represented in Figure 2. Finally, these records are applied to the finite element OpenSees model in order to perform the NLTHA and to assess the response of the components with respect to various IMs.

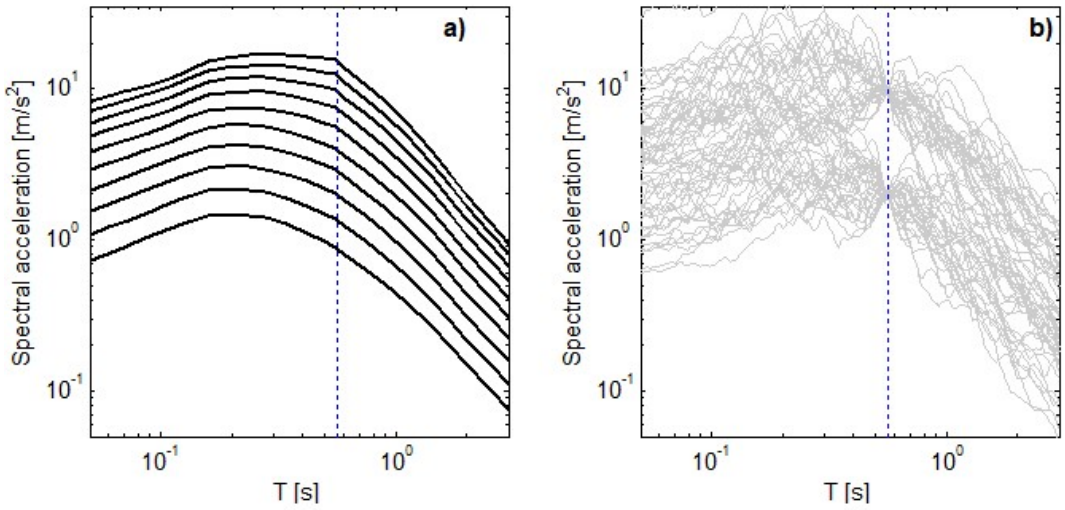

Figure 2: a) Target mean conditional spectra for the 10 scaling levels and b) Scaled respond spectra of the selected ground-motion records for two scaling levels (20% chance of exceedance within 50 years, and 5% chance of exceedance within 100 years, respectively).

Vector-based fragility functions for single NPP components

Several past studies have investigated which IMs are optimal to represent the seismic hazard loading in fragility curves (Padgett et al., 2008; Weatherill et al., 2011), through a wide range of criteria such as computability, efficiency, practicality, sufficiency, etc. While no single IM is able to fulfil all criteria simultaneously, it has been shown that the combination of two or more scalar IMs (i.e., vector-IMs) increases their predictive power (Gehl et al., 2013), with the effect of reducing the dispersion in the fragility function. To this end, it is proposed here to check the proficiency of some spectral accelerations at various periods (see Table 2): these ground-motion parameters have been selected due to their computability (i.e., availability of ground-motion prediction equations for these parameters) and their compatibility with the conditional spectrum framework, with respect to more elaborate parameters such as the cumulative absolute velocity or the Arias intensity.

Proficiency has been introduced by Padgett et al. (2008) as a composite measure of the *efficiency* (related to the dispersion β of the log*EDP* distribution as a function of log*IM*) and the *practicality* (related to the slope b of the linear relation between log*EDP* and log*IM*). It is defined as follows:

$$\zeta = \frac{\beta}{b} \quad \textbf{(1)}$$

where a small ζ implies a highly proficient IM (i.e., small dispersion and large slope).

IM	Proficiency measure ζ		
	STR	EDG1	EDG2
PGA	0.6011	**0.1137**	**0.2885**
SA(0.1s)	0.9379	0.3264	0.5559
SA(0.2s)	0.7656	0.2816	0.4279
SA(0.3s)	0.5590	0.3577	0.3875
SA(0.4s)	0.4843	0.4406	0.3798
SA(0.5s)	0.3887	0.5513	0.4010
SA(0.7s)	0.3096	0.6683	0.4282
SA(1.0s)	0.3625	0.8654	0.6268
SA(2.0s)	0.6443	1.0368	0.8328
$SA(T_1)$	**0.3049**	0.6152	0.4056
$SA(T_2)$	0.7816	0.2832	0.4371

Table 2: **Estimated proficiency measure ζ of the fragility curves for various IMs and the three component damage events considered. The highlighted terms represent the most proficient IM for each component.**

As seen from Table 2, the structural damage is well correlated with the spectral acceleration at the first vibration period of the structure, while the most proficient IM for EDGs is *PGA*. A noteworthy observation from this short analysis is that, when considering a system with various components that are represented by different types of EDPs, different IMs appear to be necessary in order to effectively account for all failure modes considered. This comment reinforces the need for using vector-IMs in this specific context, since a fragility function expressed as a function of both *PGA* and $SA(T_1)$ has the ability to appropriately model the structural damage event STR and the diesel generator failure events EDG1 and EDG2.
Therefore it is proposed to derive a vector-based fragility model for each of the three components considered. Following the well-established framework of single-IM fragility curves, the proposed model is assumed to take the following form (i.e., cumulative lognormal distribution with $PGA^{c2}.SA(T_1)^{c3}$ as a composite IM):

$$P(DS|PGA, SA[T_1]) = \frac{1}{2}[1 + erf(c_1 + c_2 \log PGA + c_3 \log SA[T_1])] \quad (2)$$

The fragility parameters c_1, c_2 and c_3 are derived from the 300 data points obtained from the NTLHA, using the limit states provided in Table 1. The maximum likelihood estimation method, as described in Shinozuka et al. (2000), is used to estimate the parameters that maximize the likelihood function *L* built with the 300 data points:

$$L(c_1, c_2, c_3) = \prod_{i=1}^{300}\left[P_{c_1,c_2,c_3}(DS|PGA, SA[T_1])\right]^{y_i}\left[1 - P_{c_1,c_2,c_3}(DS|PGA, SA[T_1])\right]^{1-y_i} \quad (3)$$

where y_i is a Boolean indicator for the damage state measured with the *i*-th ground-motion record (i.e., y_i = 1 when *DS* is reached, and 0 otherwise).
The vector-based fragility functions for all three components are displayed in Figure 3 under the form of iso-probability lines, while the corresponding fragility parameters are detailed in Table 3.

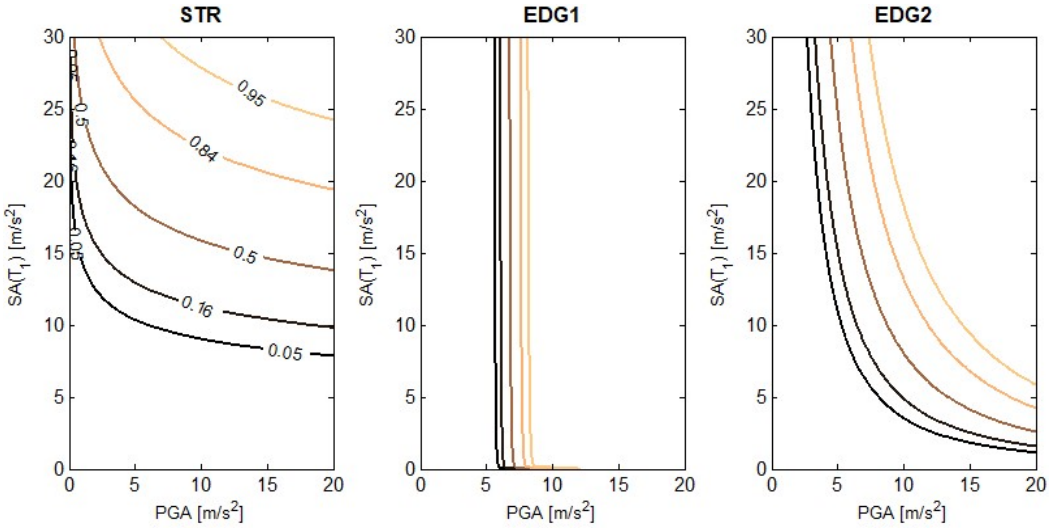

Figure 3: **Iso-probability lines (i.e., damage probabilities of 0.05, 0.16, 0.50, 0.84 and 0.95) representing the vector-based fragility functions for the three component damage events considered, with respect to *PGA* and *SA*(T_1).**

Component	Fragility parameters		
	c_1	c_2	c_3
STR	-6.651	0.414	2.063
EDG1	-12.227	6.276	0.062
EDG2	-8.299	2.322	1.417

Table 3: **Estimated fragility parameters for the three component damage events.**

The derived fragility functions confirm the preliminary analysis in Table 2, in the sense that the respective fragility functions for STR and EDG1 are mostly dependent on *SA*(T_1) and on *PGA*, respectively. On the other hand, the fragility function for EDG2 appears much more balanced between the two IMs, which is consistent with the proficiency measures for *PGA* and *SA*(T_1) having similar low values.

Vector-based fragility function for on-site power loss

The fragility functions for the component damage events are now assembled into a "system fragility function" representing the probability of occurrence of the considered system event (i.e., on-site power loss). According to the system reliability theory, this probability may be expressed as:

$$P(SYS|IM_1, IM_2) = \int_X P(SYS|IM_1, IM_2, X) f_X(x) dx$$
$$= 1 - \int_X [1 - P(DS_{STR}|IM_1, IM_2, X)][1 - P(DS_{EDG1}|IM_1, IM_2, x) P(DS_{EDG2}|IM_1, IM_2, x)] f_X(x) dx \quad \textbf{(4)}$$

where X represents a set of random variables, referred to as common source random variables (CSRVs), which are introduced in order to account for the statistical dependence between the probability of occurrence of component damage events (Kang et al., 2008). Therefore, the conditional probabilities of the component damage events become independent given $X = x$, thus greatly simplifying their combination.

As shown by Gehl and D'Ayala (2016), this system reliability problem may also be formulated through a Bayesian Network (BN), which presents the benefit of explicitly representing the sequence of events, from the hazard loading to the occurrence of the system event (see Figure 4). In the present study, the BN is used for a forward analysis (i.e., propagation of uncertainties from the top to the bottom of the direct acyclic graph); however it leaves the opportunity to perform diagnostic analyses as well (i.e.,

updating of a variable of interest, given the observation of other variables in a given state).

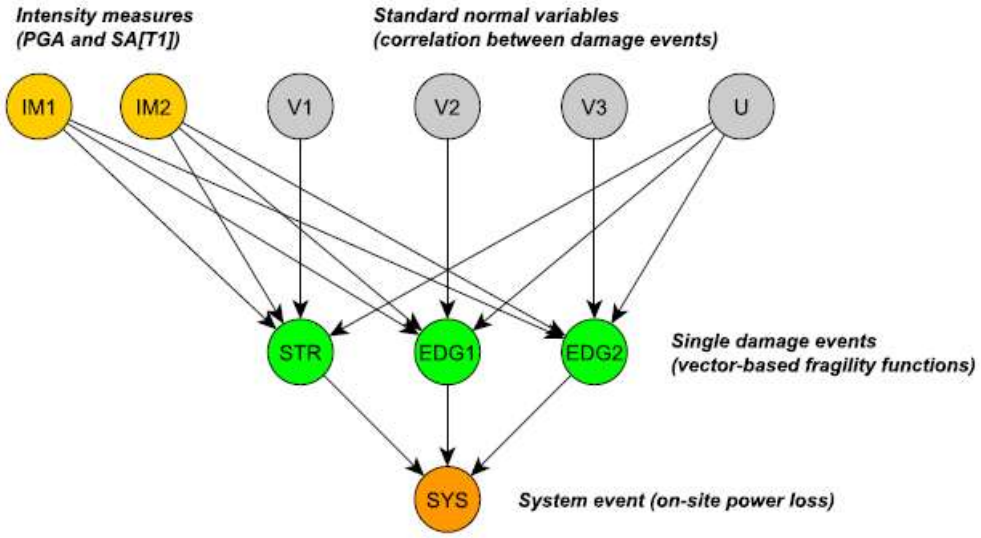

Figure 4: **Structure of the BN used to model the probability of occurrence of on-site power loss with respect to the two intensity measures *PGA* and *SA*(T_1).**

In Figure 4, each node represents a variable that is characterized by a set of discrete states and a probability table (i.e., conditional probability tables for child nodes and marginal probabilities for root nodes). The variables U, V_1, V_2 and V_3 are discretized standard normal variables that represent the CSRVs introduced in Equation 4. They result from a Dunnett-Sobel decomposition (Dunnett and Sobel, 1955), which approximates the correlation between the safety factors of the components. Thanks to this decomposition, the normalized safety factor Z_i of component i is expressed as a linear combination of standard normal variables:

$$Z_i = \sqrt{1 - t_i^2} \cdot V_i + t_i \cdot U \quad \textbf{(5)}$$

where U is the variable common to all components and V_i the variable specific to component i. The coefficient $\{t_i\}$ are estimated so that they approximate the correlation matrix between the safety factors (i.e. the correlation coefficient $\rho_{i,j} \approx t_i.t_j$ for components i and j).
The conditional probability tables of component damage events are then assembled for all possible combinations of the states of parent variables IM_1, IM_2, U and V_i. The probability of component i reaching its damage state corresponds to testing whether the safety factor F_i becomes negative:

$$P(DS_i) = P(F_i \leq 0) = P\left(Z_i \leq -\frac{\mu_F}{\sigma_F}\right) = P\left(\sqrt{1 - t_i^2} \cdot V_i + t_i \cdot U \leq -\frac{c_1 + c_2 \log PGA + c_3 \log SA[T_1]}{\sqrt{2}}\right) \quad \textbf{(6)}$$

where the mean μ_F and standard-deviation σ_F are identified with the fragility parameters derived in Equation 2 and Table 3.
Finally, the conditional probability table of the variable *SYS* is a Boolean table representing the various combinations required to reach the system event (i.e, structural damage *OR* damage to EDG1 *AND* EDG2). The BN is implemented with the Bayes Net toolbox (Murphy, 2007) and it is solved for successive combinations of IMs *PGA* and *SA*(T_1). For each value of the IM couple, the probability of the variable *SYS* reaching its damage state is computed by the BN, in order to generate a vector-based fragility function (see Figure 5).

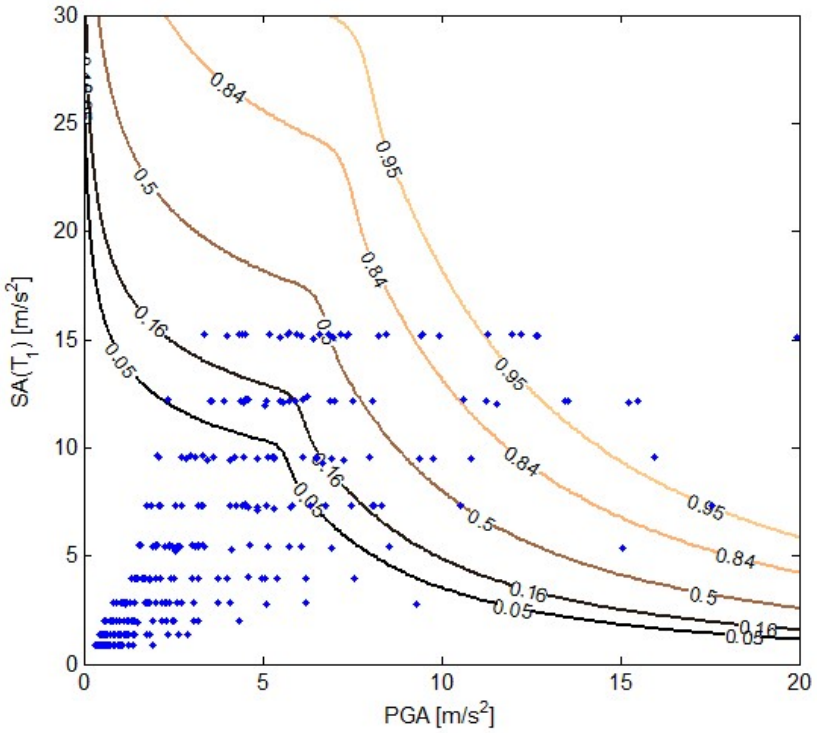

Figure 5: **Iso-probability lines representing the vector-based fragility function for the system event (on-site power loss). The blue dots represent the 300 ground-motion records that have been used in the NLTHA.**

The derived system fragility function clearly highlights the joint role of both IMs *PGA* and $SA(T_1)$ in the assessment of the on-site power loss. For instance, for low *PGA* values and high $SA(T_1)$ values, an edge effect is observed, where the structural failure mode is dominating; while the functional failure of both EDGs appears to be the main damage mechanism when larger *PGA* values are reached.
The sampling space covered by the 300 ground-motion records is also represented in Figure 5: this information is essential to apprehend the limits of the proposed fragility model, as extreme configurations of *PGA* and $SA(T_1)$ are very unlikely. However, since this fragility model is meant to be used in a PSA for a given NPP site, the ground-motion selection procedure based on conditional spectrum ensures that the joint distribution of the vector-IMs is consistent with the expected hazard level.

Robustness of the proposed fragility model

In order to assess the benefit of using a vector-based fragility model, it is proposed to compare with other scalar or vector-IM fragility functions that have been derived using exactly the same ground-motion records and NTLHA outcomes. The three benchmarked models are described as follows:

- Model *a*: derivation of single-IM fragility curves for components, with $SA(T_1)$ for STR and *PGA* for EDG1 and EDG2; the sub-system fragility model is still represented as a vector-based distribution, as a function of *PGA* and $SA(T_1)$.
- Model *b*: derivation of single-IM fragility curves for components, using *PGA* for all curves; the sub-system fragility model therefore becomes a scalar-based distribution, as a function of *PGA* only.
- Model *c*: derivation of single-IM fragility curves for components, using $SA(T_1)$ for all curves; the sub-system fragility model therefore becomes a scalar-based distribution, as a function of $SA(T_1)$ only.

These alternative models are represented in Figure 6 and they are superimposed with the 5%-95%

confidence bounds of the [*PGA* - *SA*(T_1)] distribution of the ground-motion records, so that the area between these bounds corresponds to the expected hazard loading (in terms of correlation between *SA*(T_1) and *PGA*) for the studied site). Within this area, it is worth noting that models *b* and *c* show completely different behaviours, as expected due to the choice of a scalar IM. On the other hand, model *a* appears quite similar to the proposed model in Figure 5, where the same "corner effect" may be observed: outside the confidence area, however, the models become very different, due to the inability of model *a* to account for combinations of *PGA* and *SA*(T_1) at the component level.

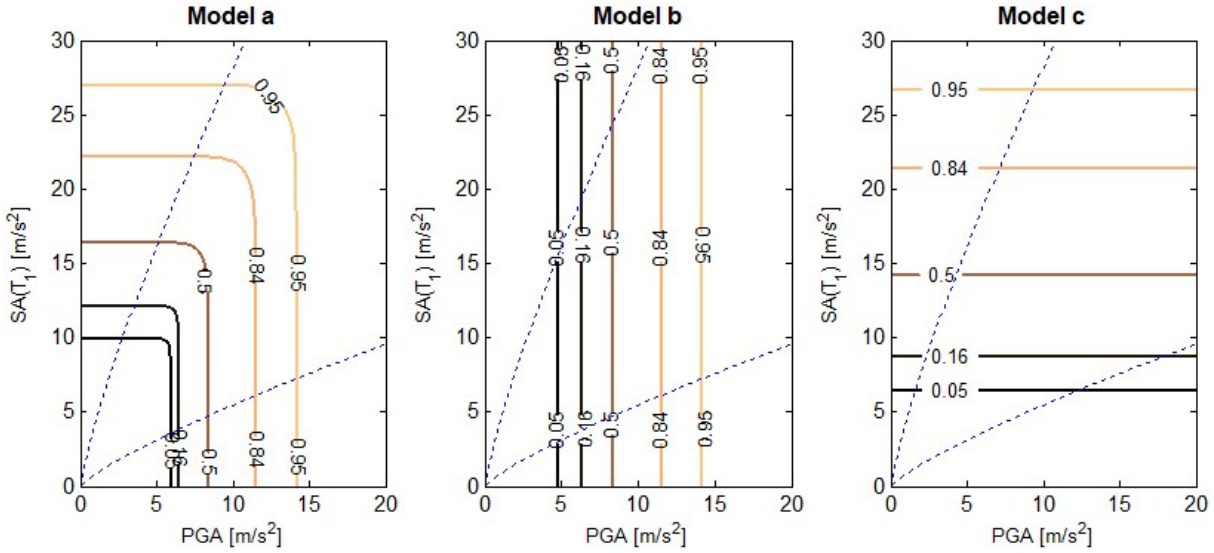

Figure 6: **Iso-probability lines representing the fragility functions for the system event (on-site power loss) in the [*PGA* – *SA*(T_1)] space, for the three alternative models considered. The dotted blue lines represent the 5%-95% confidence intervals of the space covered by the 300 ground-motion records.**

In complement to this qualitative exploration of the models, the Akaike Information Criterion (AIC) is then introduced as way to quantitatively assess the goodness-of-fit of the various models. The AIC accounts for the number of parameters used in a model through the variable *k*, in order to penalize the over-parametrization of some models. It is expressed as follows:

$$\mathrm{AIC} = 2k - 2\log L \qquad \textbf{(7)}$$

where *L* is the likelihood function of the model, which is computed as a product of the 300 conditional probabilities corresponding to the 300 ground-motion records. The resulting AIC values for the four models (i.e., the proposed vector-based model and the three alternative models) are detailed in Table 4.

Fragility model	Nb of parameters *k*	AIC
Proposed model	9	97.0
Model *a*	6	97.6
Model *b*	6	111.7
Model *c*	6	150.7

Table 4: AIC values for the various fragility models considered, with respect to the 300 ground-motion records.

As expected, models *b* and *c* are associated with a large loss of information (i.e., high AIC), while the proposed model and model *a* are very close, although the AIC from model *a* remains slightly higher. The proposed model requires 9 parameters (i.e., 3 coefficients c_1, c_2 and c_3 for each of the 3 component

fragility functions), which results in a greater penalty than for model *a* (only 6 parameters needed, 2 for each single-IM fragility function): this partly explains why their AIC values are so close, even if the term linked to the likelihood *L* is smaller for the proposed model. Finally, because the AIC for the proposed model is not larger than the AIC for model *a* even with the parameter penalty, one may argue that the proposed model is not likely to be grossly over-parametrized.
Since the results in Table 4 are inconclusive regarding the most informative model, a cross-validation procedure is adopted, where one ground-motion record is randomly taken out from each scaling bins: 100 random samples are thus generated, containing 290 records each (i.e. 10 scaling bins multiplied by 29 records, instead of 30). Each of the sampled sub-sets is then used to generate the fragility models and to compute the corresponding AIC values: the distributions of the AIC values for all sub-sets, referred to as AIC*, are displayed in Figure 7 for the two candidate models.

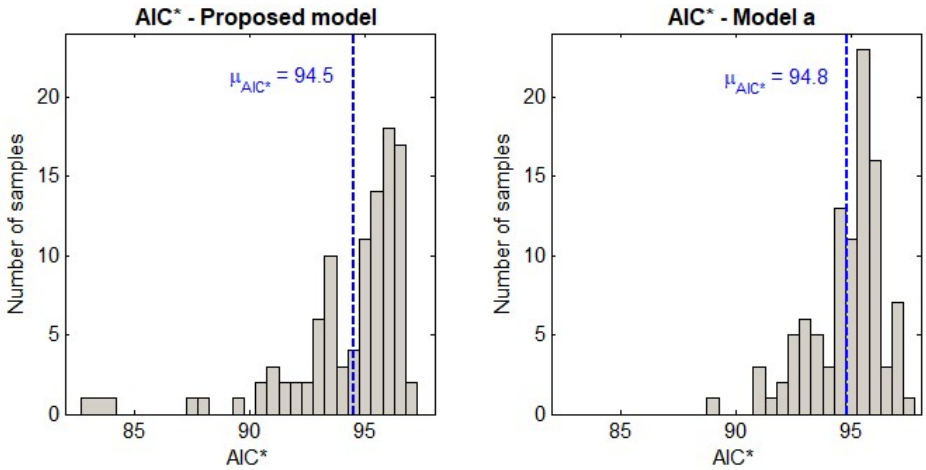

Figure 7: AIC values derived from a cross-validation procedure for two competing fragility models considered, with respect to the 300 ground-motion records. Blue vertical line corresponds to the mean value.

The histograms in Figure 7 show that the AICs of the proposed model tend to be slightly lower than for model *a*, although the differences are very low. Therefore, considering vector-based fragility functions at the component level does not present a significant improvement from single-IM component fragility functions: this observation is mostly due to the hazard-consistent ground-motion selection procedure that has been adopted here, which ensures that the correlation between accelerations at different periods is well constrained (thus minimizing the impact of using vector IMs). On the other hand, the vector-based fragility function at the system level (i.e. model *a*) proves to be a much more robust model than the use of single-IM fragility functions to represent the system failure (i.e. models *b* and *c*). Therefore, the benefit of using vector IMs is especially noticeable when the damage of several components is assessed through different types of EDPs, as in the present specific case: when sub-systems of different types of components are considered, Bayesian networks based on the system reliability framework are able to use single-IM component fragility functions and to build more complex probability distribution that are able to account for various types of loadings, in terms of amplitude or frequency content.

Conclusion

This study has investigated the application of vector-based fragility functions to the assessment of the failure probability of a NPP sub-system, namely the emergency generation of on-site power. A vector-IM containing *PGA* and *SA* at the fundamental period of the structure has been identified as proficient intensity measure for the derivation of the three component fragility functions. However, when using single-IM fragility functions at the component level and assembling their respective contributions at the system level (i.e. model *a*), it has been found that the benefit of deriving vector-based fragility functions already at the component level is not significant, as long as the seismic hazard loading remains within

the range of ground-motion records that have been used in the NLTHA. The ground-motion selection procedure based on conditional spectrum ensures the hazard consistency of the inputs, which tends to account partially for the correlation between the spectral ordinates. As a result, the computation of the AIC for the various models considered has revealed that the vector-based fragility functions at the component level are close to overfitting the data, when compared to model *a*. This conclusion should however be confirmed through the study of more complex structures, where other modes of vibrations could play a larger role. Moreover, the availability of a larger number of natural ground motions during the conditional spectra selection procedure would also help to broaden the record-to-record variability, thus potentially giving more weight to the vector-IM assumption.
Nevertheless, this work has shown that it is possible to combine several IMs at the system level, when the objective of the derived fragility function is to assess the probability of occurrence of a given system event (e.g. failure of the on-site emergency power). To this end, the proposed Bayesian Network formulation is an accurate tool to represent the dependencies between variables (e.g. hazard loading, component damage states, system damage state) and to reproduce the statistical dependence between component damage events, following the well-established system reliability framework. While this study has been applied to vector-IMs representing various features of the seismic hazard loading, it is expected to expand this approach to the multi-hazard fragility and human reliability assessment of NNP components and sub-systems: in that case, the different susceptibility of various components to different types of hazard loadings will require the combination of several IMs in order to accurately capture all possible failure modes in the system.

Acknowledgment

This study has been carried out within the NARSIS project, which has received funding from the European Union's H2020-Euratom Programme under grant agreement N° 755439. The Pacific Earthquake Engineering Research Center is gratefully acknowledged for providing access to their database of ground-motion records.

References

1) P. Bazzurro and A.C. Cornell, "Disaggregation of seismic hazard," *Bulletin of the Seismological Society of America*, **89**, 2, 501-520 (1999).
2) Y.S. Choun, M.K. Kim and Y. Ohtori, "The use of a base isolation system for an emergency diesel generator to reduce the core damage frequency caused by a seismic event", *19th International Conference on Structural Mechanics in Reactor Technology (SMiRT 19)*, Toronto, Canada (2007).
3) C.W. Dunnett and M. Sobel, "Approximations to the probability integral and certain percentage points of a multivariate analogue of Student's t-distribution," *Biometrica*, 42, 1-2, 258–60 (1955).
4) P. Gehl and D. D'Ayala, "Development of Bayesian Networks for the multi-hazard fragility assessment of bridge systems," *Structural Safety*, **60**, 37-46 (2016).
5) P. Gehl, D. Seyedi and J. Douglas, "Vector-valued fragility functions for seismic risk evaluation," Bulletin of Earthquake Engineering, **11**, 2, 365-384 (2013).
6) N. Jayaram, T. Lin and J.W. Baker, "A computationally efficient ground-motion selection algorithm for matching a target response spectrum mean and variance," *Earthquake Spectra*, **27**, 3, 797-815 (2011).
7) W.H. Kang, J. Song and P. Gardoni, "Matrix-based system reliability method and applications to bridge networks," *Reliability Engineering and System Safety*, **93**, 1584-1593 (2008).
8) T. Lin, C. Haselton and J.W. Baker, "Conditional spectrum-based ground motion selection. Part I," *Earthquake Engineering and Structural Dynamics*, **42**, 12, 1847-1865 (2013).
9) F. McKenna, G.L. Fenves and M.H. Scott, *Open system for earthquake engineering simulation*, Technical report, Pacic Earthquake Engineering Research Center, University of California, Berkeley, California (2000).
10) A. Modica and P.J. Stafford, "Vector fragility surfaces for reinforced concrete frames in Europe," *Bulletin of Earthquake Engineering*, **12**, 4, 1725-1753 (2014).
11) K. Murphy, *Bayes Net Toolbox*, Available from: https://github.com/bayesnet/bnt (2007).
12) NUREG, *Reevaluation of station blackout risk at nuclear power plants – Analysis of station blackout risk*, U.S. Nuclear Regulatory Commission, NUREG/CR-6890, Vol. 2 (2005).

13) J.E. Padgett, B.G. Nielson and R. DesRoches, “Selection of optimal intensity measures in probabilistic seismic demand models of highway bridge portfolios,” *Earthquake Engineering and Structural Dynamics*, **37**, 5, 711-725 (2008).
14) PEER, *PEER NGA-West2 Database*, Pacific Earthquake Engineering Research Center (2013).
15) A.S. Pisharady and P.C. Basu, “Seismic fragility of a civil engineering structure,” *20th International Conference on Structural Mechanics in Reactor Technology (SMiRT 20)*, Espoo, Finland (2009).
16) M. Shinozuka, Q. Feng, J. Lee and T. Naganuma, “Statistical analysis of fragility curves,” *Journal of Engineering Mechanics*, 126, 1224-1231 (2000).
17) L. Sousa, V. Silva, M. Marques, H. Crowley and R. Pinho, “Including multiple IMTs in the development of fragility functions for earthquake loss estimation,” *2nd International Conference on Vulnerability and Risk Analysis and Management*, Liverpool, UK (2014).
18) Z Wang, *Seismic Risk Analysis for Nuclear Energy Facilities*, PhD Thesis, University of Waterloo, Ontario, Canada (2015).
19) G. Weatherill, H. Crowley and R. Pinho, *Efficient intensity measures for components within a number of infrastructures*, FP7 SYNER-G Deliverable Report D2.12 (2011).
20) J. Woessner, L. Danciu, P. Kaestli, and D. Monelli, *Database of seismogenic zones, Mmax, earthquake activity rates, ground motion attenuation relations and associated logic trees*, FP7 SHARE Deliverable Report D6.6 (2013).
21) I. Zentner, M. Gündel and N. Bonfils, “Fragility analysis methods: Review of existing approaches and application,” *Nuclear Engineering and Design*, **323**, 245-258 (2017).